



**A new model for the
global
biogeochemical cycle
of carbonyl sulfide**

T. Launois et al.

**A new model for the global
biogeochemical cycle of carbonyl sulfide
– Part 1: Assessment of direct marine
emissions with an oceanic general
circulation and biogeochemistry model**

T. Launois¹, S. Belviso¹, L. Bopp¹, C. G. Fichot², and P. Peylin¹

¹Laboratoire des Sciences du Climat et de l'Environnement (LSCE Saclay), IPSL, CEA, CNRS, UVSQ, CE Saclay, Bât 703 L'Orme des Merisiers, 91191, Gif-sur-Yvette, France

²Jet Propulsion Laboratory, California Institute of Technology, Pasadena, California, USA

Received: 22 May 2014 – Accepted: 17 July 2014 – Published: 11 August 2014

Correspondence to: T. Launois (thomas.launois@lsce.ipsl.fr)

Published by Copernicus Publications on behalf of the European Geosciences Union.

Title Page

Abstract

Introduction

Conclusions

References

Tables

Figures



Back

Close

Full Screen / Esc

Printer-friendly Version

Interactive Discussion



Abstract

The global budget of tropospheric carbonyl sulfide (OCS) is believed to be at equilibrium because background air concentrations have remained roughly stable over at least the last decade. Since the uptakes of OCS by leaves (associated to photosynthesis) and soils have been revised significantly upwards recently, an equilibrated budget can only be obtained with a compensatory source of OCS. It has been assumed that the missing source of OCS comes from the low latitude ocean, following the incident solar flux. The present work uses parameterizations of major production and removal processes of organic compounds in the NEMO-PISCES Ocean General Circulation and Biogeochemistry Model to assess the marine source of OCS. In addition, the OCS photo-production rates computed with the NEMO-PISCES model were evaluated independently using UV absorption coefficient of chromophoric dissolved organic matter (derived from satellite ocean color) and apparent quantum yields available in the literature. Our simulations show global direct marine emissions of COS in the range of 573–3997 Gg S yr⁻¹, depending mostly on the quantification of the absorption rate of chromophoric dissolved organic matter. The high estimates on that range are unlikely, as they correspond to a formulation that most likely overestimate photo-production process. Low and medium (813 Gg S yr⁻¹) estimates derived from the NEMO-PISCES model are however consistent spatially and temporally with the suggested missing source of Berry et al. (2013), allowing thus to close the global budget of OCS given the recent estimates of leaf and soil OCS uptakes.

1 Introduction

Carbonyl sulfide (OCS) is a long-lived sulfur-containing trace gas with direct and indirect effects on the radiation budget of the atmosphere (OCS being both a tropospheric greenhouse gas and a source of sulfur aerosols to the stratosphere). But these radiative effects are low compared to the radiative forcings of greenhouse gases (GHG)

A new model for the global biogeochemical cycle of carbonyl sulfide

T. Launois et al.

Title Page

Abstract

Introduction

Conclusions

References

Tables

Figures



Back

Close

Full Screen / Esc

Printer-friendly Version

Interactive Discussion



A new model for the global biogeochemical cycle of carbonyl sulfide

T. Launois et al.

[Title Page](#)

[Abstract](#)

[Introduction](#)

[Conclusions](#)

[References](#)

[Tables](#)

[Figures](#)



[Back](#)

[Close](#)

[Full Screen / Esc](#)

[Printer-friendly Version](#)

[Interactive Discussion](#)



and tropospheric aerosols of anthropogenic origin (Brühl et al., 2012 and references therein). But because OCS is the most abundant sulfur-containing gas in the atmosphere, it contributes for a large portion to the stratospheric sulfate layer during volcanically quiescent periods (Notholt et al., 2003). OCS also participates in some key reactions within the global carbon cycle, especially reactions associated with leaf photosynthesis and soil microbial activities (Berry et al., 2013 and references therein). As such, it holds great promises for the studies of plant physiology, terrestrial ecosystem production and the global carbon cycle thanks to its potential use as a tracer for canopy photosynthesis, transpiration and stomatal conductance (Wohlfahrt et al., 2012 and references therein).

Measurements of OCS from the global air-monitoring network of the National Oceanic and Atmospheric Admistration (NOAA) provided compelling evidence for the existence of a major sink of this gas in the continental boundary layer, mainly attributed to biospheric uptake (Montzka et al., 2007; Campbell et al., 2008). The uptake of OCS by plants was originally modeled to be no more than a few hundreds of Gg S yr^{-1} (Kettle et al., 2002), but it has been recently revised upwards (Montzka et al., 2007; Suntharalingam et al., 2008; Berry et al., 2013). Soils could also play a role in the budget of OCS. It is still a strong matter of debate but recent estimates suggest that much more OCS is taken up by soils than initially proposed (few hundred of Gg S yr^{-1} ; Berry et al., 2013). Since background air concentrations have remained roughly stable over at least the last decade (Montzka et al., 2007), the global budget of tropospheric OCS is believed to be at equilibrium. Kettle et al. (2002) proposed an initial global budget of OCS with ocean and anthropogenic sources compensating for the main uptake by vegetation. However, because deposition fluxes of OCS to vegetation and soils are much higher than proposed initially, an equilibrated budget can only be obtained with a compensatory source of OCS. Berry et al. (2013) assume that the missing source of OCS comes from the oceans. This missing source has been inferred through a simple inversion approach that optimizes sources and sinks based on global measurements of atmospheric OCS levels collected in the NOAA network. This inversion pointed towards

a larger global oceanic source of OCS with higher proportions of tropical emissions than previously established.

The ocean is believed to be the largest source of atmospheric OCS (Chin and Davis, 1993, 2002; Berry et al., 2013). It contributes to OCS in the troposphere by direct emission of this gas, and by large emissions of carbon disulfide (CS₂) and dimethylsulfide (DMS) quickly oxidized into OCS (with an approximate lifetime of 1 day) (Koch et al., 1999; Chin et al., 2000; Kloster, 2006). However, estimates of sea–air fluxes of OCS and their spatial distributions remain largely unknown. Kettle et al. (2002) simulated direct global oceanic OCS fluxes from –110 Gg S yr⁻¹ (a sink) to 190 Gg S yr⁻¹ (a source to the atmosphere), while previous estimates based on field observations suggested global direct oceanic OCS emissions from 160 to 640 Gg S yr⁻¹ (Chin and Davis, 1993; Watts, 2000). Both studies suggested sea–air OCS emissions mainly take place at mid and high latitudes.

OCS concentrations in the ocean sub-surface show a strong diurnal cycle with a mid-afternoon maximum, suggesting that photo-production is a major source of marine OCS (Ferek and Andreae, 1984; Xu et al., 2001; von Hobe et al., 2003). In addition, OCS can also be produced in marine waters when no light is available. This pathway is therefore called dark-production. Its rate seems proportional to the amount of organic material, and has therefore so far been linked to the chromophoric dissolved organic matter (CDOM) absorption coefficient (von Hobe et al., 2001, 2003). Finally, OCS surface concentrations and fluxes are also strongly influenced by the continuous temperature- and pH-dependent hydrolysis of OCS to carbon dioxide (CO₂) and hydrogen sulfide (H₂S) (von Hobe et al., 2003).

The present work reassesses the marine source of OCS using the 3D oceanic NEMO-PISCES Ocean General Circulation and Biogeochemistry model with process-based parameterizations of the main OCS production and removal processes (Fig. 1). The present study proposes two independent approaches to quantify the photo-production of OCS. The dark-production rate implemented in the NEMO-PISCES model follows the formulation of von Hobe et al. (2001, 2003). Therefore, the

A new model for the global biogeochemical cycle of carbonyl sulfide

T. Launois et al.

Title Page

Abstract

Introduction

Conclusions

References

Tables

Figures



Back

Close

Full Screen / Esc

Printer-friendly Version

Interactive Discussion



dark-production rate, even if supposed to be light-independent, is linked to the chromophoric dissolved organic matter absorption coefficient at 350 nm (a_{350}), as the variable provides an indirect estimate of the seawater richness in organic matter.

As parameterizations found in literature for both dark- and photo-production of OCS are related to the UV absorption coefficient of CDOM at 350 nm, sensitivity tests are performed using three different formulations for this variable. Sensitivity tests are also performed on hydrolysis, exploring two different formulations. In the result section, vertical profiles and global maps of OCS concentrations and OCS sea–air fluxes obtained with the NEMO-PISCES model are compared with in-situ measurements. Finally, the quantities and spatial distributions of global OCS emissions modeled in the present work are evaluated against previous global estimates.

2 Methods

2.1 Description of NEMO-PISCES and experimental design

In this study, we use the Pelagic Interaction Scheme for Carbon and Ecosystem Studies (PISCES) ocean biogeochemical model. As a detailed description of the model parameterizations is given in Aumont and Bopp (2006), the model is only briefly presented here. The model has 24 compartments, including four living pools: two phytoplankton size classes/groups (nanophytoplankton and diatoms) and two zooplankton size classes (microzooplankton and mesozooplankton). Phytoplankton growth can be limited by five different nutrients: nitrate, ammonium, phosphate, silicate and iron. The internal concentrations of chlorophyll for both phytoplankton groups are prognostically simulated with Chlorophyll-to-Carbon ratios computed as a function of light and nutrient stress. There are three nonliving compartments: semi-labile dissolved organic matter (with remineralization timescales of several weeks to several years), small and large sinking particles. In addition to the version of the model used in Aumont and Bopp

A new model for the global biogeochemical cycle of carbonyl sulfide

T. Launois et al.

Title Page

Abstract

Introduction

Conclusions

References

Tables

Figures



Back

Close

Full Screen / Esc

Printer-friendly Version

Interactive Discussion



(2006), we also include here a prognostic module computing OCS concentrations in seawater.

PISCES is coupled to the general circulation model Nucleus for European Modelling of the Ocean (NEMO, Madec et al., 1998). A release of the model is available for the community (<http://www.nemo-ocean.eu/>). Here, we use the global configuration ORCA2 with a resolution of $2^\circ \times 0.5\text{--}2^\circ$ and 31 vertical levels (with a ~ 10 m-resolution in the first 200 m). NEMO-PISCES is first run 3000 years to obtain an equilibrated state, forced in offline mode by the Consortium for Oceanic Research and Education (CORE2) Normal Year Forcing, (Large and Yeager, 2008) and initialized with climatological nutrient data. The OCS module is then only run two additional years as it converges towards equilibrium much more rapidly. The results presented in this study correspond to the last year of this simulation.

2.2 Parameterizations of OCS production and removal processes implemented in NEMO-PISCES

The clear diurnal cycle of sea-surface OCS concentrations with peak values during mid-afternoon suggests photochemical processes play an important role in the production of OCS. Organo-sulfur compounds with thiol groups (-SH), such as cysteine and methyl mercaptans (CH_3SH), have been suggested as OCS precursors (Ferek and Andreae, 1984; Flöck et al., 1997; Ulshöfer et al., 1996). Moreover, measured CH_3SH diurnal cycles were coherent with the hypothesis that its photo-destruction could lead to OCS production (Xu et al., 2001). Because no global map of CH_3SH is available, we followed parameterizations of OCS photo-production found in literature which relate photo-production rate of OCS to the UV irradiance intensity at the sea surface and to the efficiency of chromophoric dissolved organic matter (CDOM) available to absorb this UV radiation. The quantification of this photochemical process can be amenable to remote sensing because of its critical dependence on ocean UV and visible optical properties. Additional parameterizations were needed to complete the description of OCS formation and destruction processes in NEMO-PISCES. We therefore

implemented specific modules to calculate the formation of OCS via dark-production (a light-independent pathway) and the hydrolysis rate of OCS in sea waters. Finally, air–sea exchanges of OCS were described in an analogous way to Fick’s diffusion law.

2.2.1 UV light penetration in seawater

5 Surface irradiance received at each grid point is a function of cloud coverage. Deduced surface UV irradiance is taken equal to 4.4 % of the total light received at sea surface. UV penetration at depth in marine waters in NEMO-PISCES was taken equal to the penetration calculated with the deep blue wavelength for visible light attenuation coefficient. As this is a rough approximation and might lead to over-estimating maximum
10 depth penetration for UV irradiance, we set the UV value to zero for layers deeper than 30 m, which corresponds to the average depth at which less than 10 % of surface UV irradiance penetrates for marine waters containing less than 1 mg m^{-3} of chlorophyll (Bricaud et al., 1995; Tedetti et al., 2007).

2.2.2 Parameterization of CDOM absorption coefficient at 350 nm (a_{350})

15 Chromophoric (or colored) dissolved organic matter (CDOM) is the fraction of the dissolved organic matter that absorbs light, ranging from ultraviolet to visible wavelengths. Its concentration increases in seawater with important biological production rates and elevated terrestrial inputs. Its concentration decreases with photochemical degradation and microbial consumption. CDOM distribution is also controlled by the deep ocean circulation, upwelling and/or vertical mixing (Para et al., 2010 and references therein).
20 CDOM absorbs part of available light, therefore negatively impacting primary productivity of aquatic ecosystems. However, as provider of a substitute for microbial respiration, photo-degraded CDOM positively impact the secondary productivity of the oceanic ecosystems. CDOM has been identified one of the most impacting factor to control UV
25 attenuation in waters.

A new model for the global biogeochemical cycle of carbonyl sulfide

T. Launois et al.

Title Page

Abstract

Introduction

Conclusions

References

Tables

Figures



Back

Close

Full Screen / Esc

Printer-friendly Version

Interactive Discussion



A new model for the global biogeochemical cycle of carbonyl sulfide

T. Launois et al.

Title Page

Abstract

Introduction

Conclusions

References

Tables

Figures

◀

▶

◀

▶

Back

Close

Full Screen / Esc

Printer-friendly Version

Interactive Discussion



As the calculation of CDOM concentration in NEMO-PISCES was not possible due to insufficient knowledge and parameterization on the controlling processes, its absorption at 350 nm (a_{350}) was chosen to quantify CDOM quantities, as done in Para et al. (2010). Therefore, a_{350} provides information on the available UV-light quantities, primordial for the photo-production of OCS, and simultaneously provides indirect information on the CDOM quantities, thus the organic matter richness of the waters, primordial for dark-production estimates. Since a_{350} is of central importance in our simulations, sensitivity tests were performed using three different a_{350} formulations.

Morel and Gentili (2009) and Preiswerk et al. (2000) deduced CDOM absorption coefficients at a given wavelength from in situ measurements, and then extrapolated the absorption coefficient of CDOM at 350 nm by using the following standard exponential relation:

$$a_{\text{CDOM}}(\lambda) = a_{\text{CDOM}}(\text{ref}) \times e^{(-S \times (\text{ref} - \lambda))} \quad (1)$$

where S is the spectral slope coefficient of CDOM between λ and the reference wavelength (ref).

a_{350} from Morel and Gentili (2009)

The parameterization of a_{350} from Morel and Gentili (2009) is based on spectral reflectances of the ocean over Case 1 waters. Case 1 waters are those for which the optical properties of CDOM closely follow the optical properties of phytoplankton, as defined in Morel (1988). Spectral reflectances were derived from ocean color remote sensing data at several wavelengths to allow separation between CDOM and chlorophyll reflectance signatures. Deduced relation between CDOM absorption coefficient and chlorophyll concentration has been established by remote-sensing on Case 1 waters as:

$$a_{\text{CDOM}}(400) = 0.065[\text{Chl}]^{0.63} \quad (2)$$

a_{350} from Preiswerk et al. (2000)

The second parameterization was taken from Preiswerk et al. (2000) who deduced a_{350} from modeled CDOM absorption coefficient at 440 nm. To model a_{440} , satellite ocean color data were used as a proxy for chlorophyll concentration and combined with the relation of Garver and Siegel (1998), Eq. (3):

$$\text{per}(a_{440}) = -26[\log(\text{chl})] + 26 \quad (3)$$

$$a_{\text{PH},440} = 0.0448 \text{ chl} \quad (4)$$

$$\text{per}(a_{440}) = \frac{a_{440}}{a_{\text{PH},440} + a_{440}} \times 100\% \quad (5)$$

where $a_{\text{PH},440}$ is the absorption coefficient of the phytoplankton at 440 nm, and $\text{per}(a_{440})$ is the percent of the total non-seawater absorption coefficient at 440 nm (due to CDOM).

a_{350} from MODIS Aqua ocean color

A relationship between a_{350} and chlorophyll a was developed in this study using MODIS Aqua ocean color data collected continuously between July 2002 and July 2010. Monthly climatologies of MODIS Aqua chlorophyll a surface concentrations were used, and MODIS Aqua remote-sensing reflectances were used to derive corresponding monthly climatologies of a_{350} for the global surface ocean. The SeaUV algorithm developed by Fichot et al. (2008) was used to estimate the diffuse attenuation coefficient at 320 nm, $K_d(320)$, from the remote-sensing reflectances. A ratio $a_{\text{CDOM}}(320)/K_d(320) = 0.68$ derived from an extensive set of in situ measurements was then used to calculate the absorption coefficient of CDOM at 320 nm, a_{320} , from $K_d(320)$ (Fichot and Miller, 2010). A spectral slope coefficient of 0.0198 derived from the same in situ data set was then used to calculate a_{350} from a_{320} using Eq. (1).

The a_{350} data from the twelve monthly climatologies were regressed on the corresponding MODIS Aqua chlorophyll a concentrations using the fourth-order polynomial

A new model for the global biogeochemical cycle of carbonyl sulfide

T. Launois et al.

Title Page

Abstract

Introduction

Conclusions

References

Tables

Figures

◀

▶

◀

▶

Back

Close

Full Screen / Esc

Printer-friendly Version

Interactive Discussion



shown in Eq. (6).

$$\ln(a_{350}) = 0.5346C - 0.0263C^2 - 0.0036C^3 + 0.0012C^4 - 1.6340 \quad (6)$$

where $\ln([\text{Chl}])$, and $[\text{Chl}]$ has units of mg m^{-3} , and a_{350} has units of m^{-1} .

2.2.3 OCS photo-production rates as modeled in NEMO-PISCES

OCS photo-production is primarily induced by the interaction of UV radiation and natural photosensitizers in CDOM (Ferek and Andreae, 1984; Flöck et al., 1997). Therefore, Uher et al. (1997) photo-production parameterization takes into account the incident UV irradiance and OCS production efficiency (apparent quantum yield, AQY). An AQY represents the spectral efficiency of a photochemical process (e.g., photochemical production of OCS), and is generally determined in the laboratory by normalizing the quantity of OCS produced during solar exposure to the amount of photons absorbed by CDOM during that same solar exposure. Since measurements of AQY showed large variations depending on the location and the season, the authors decided to normalize the measured AQY by the absorption coefficient of CDOM available for the reaction at the same location. Therefore, the relation obtained in North Sea water for offshore measurements is the following:

$$P = 2.1UV a_{350} \quad (7)$$

where P is the OCS photo-production rate ($\text{pmol m}^{-3} \text{s}^{-1}$), UV is the incident irradiance integrated from 295 to 385 nm (W m^{-2}). The 2.1 coefficient comes from normalization of measured photoproduction constants by measured CDOM absorption coefficient values at 350 nm, and has a unit of $\text{fmol L}^{-1} \text{s}^{-1} \text{W}^{-1} \text{m}^3$.

2.2.4 Parameterization of OCS dark-production rates

Dark-production efficiency relies on available organic matter. Microbial activities are suggested as main precursors for the OCS dark-production pathway, but their exact

A new model for the global biogeochemical cycle of carbonyl sulfide

T. Launois et al.

Title Page

Abstract

Introduction

Conclusions

References

Tables

Figures



Back

Close

Full Screen / Esc

Printer-friendly Version

Interactive Discussion



and its temperature, following respectively:

$$k_{\text{hydr_Kamyshny}} = e^{(24.3 - \frac{10450}{T})} + \frac{k_w}{[\text{H}^+]} e^{(22.8 - \frac{6040}{T})} \quad (T \text{ in K}) \quad (9a)$$

$$k_{\text{hydr_Elliott}} = 4.19 \times 10^{-12} e^{(-\frac{12110}{T})} + \frac{k_w}{[\text{OH}^-]} 1.41 \times 10^{18} e^{(-\frac{-11580}{T})} \quad (T \text{ in K}) \quad (9b)$$

5 With k_w the ion product of marine water, $[\text{OH}^-]$ and $[\text{H}^+]$ the OH^- and H^+ activities.

Both hydrolysis constant rates, as function of temperature, are represented in the case of pH = 8.2 in Fig. 2.

2.2.6 OCS sea-to-air fluxes

10 OCS exchange between the ocean and the atmosphere can be described in an analogous way to Fick's diffusion law. The sea-air OCS flux depends on the OCS concentration in sea water and the partial pressure of OCS in air:

$$F_{\text{OCS}} = k_{\text{water}} \left([\text{OCS}]_{\text{aq}} - \frac{[\text{OCS}]_{\text{atm}}}{H} \right) \quad (10)$$

15 where F_{OCS} is the sea-air flux ($\text{pmol m}^{-2} \text{s}^{-1}$), $[\text{OCS}]_{\text{aq}}$ and $[\text{OCS}]_{\text{atm}}$ are the OCS concentration at sea surface and in the atmosphere respectively (in pmol m^{-3}). The atmospheric OCS concentration $[\text{COS}]_{\text{atm}}$ over sea surface was constantly imposed, assuming an atmospheric mixing ratio of 500 ppt. Through H , the Henry's law constant, the sea-air OCS flux also depends on temperature, calculated following Johnson et al. (1986):

$$20 \quad H = e^{(12722 - \frac{3496}{T})} \quad (T \text{ in K}) \quad (11)$$

k_{water} is the piston velocity (in m s^{-1}) for OCS. The coefficient is deduced from the Schmidt number of OCS and depends on surface wind speed, and is calculated with

20688

Title Page

Abstract

Introduction

Conclusions

References

Tables

Figures

⏪

⏩

◀

▶

Back

Close

Full Screen / Esc

Printer-friendly Version

Interactive Discussion



the relation of Wanninkhof (1992):

$$k_{\text{water}} = [0.3u^2 + 2.5 \times (0.5246 + 0.016256T + 0.00049946T^2)] \times \sqrt{\frac{660}{S_{\text{OCS}}}} (T \text{ in } ^\circ\text{C}) \quad (12)$$

where u is the wind speed (in m s^{-1}).

Note that Kettle et al. (2002) used similar parameterizations for the sea-surface exchange coefficient and the same relation from Wanninkhof et al. (1992) to model the global OCS flux at sea surface than the ones presented in this work.

S_{OCS} is the Schmidt number for OCS (dimensionless), deduced as suggested by Ullshöfer (1995) from kinetic viscosity (ν) and diffusion coefficient (D) (both in $\text{m}^2 \text{s}^{-1}$), respectively derived from:

$$S_{\text{OCS}} = \frac{\nu}{D} \quad (13)$$

with:

$$\nu = (1.792747 - 5.126103 \times 10^{-2}T + 5.918645 \times 10^{-4}T^2) \times 1 \times 10^{-6} (T \text{ in } ^\circ\text{C}) \quad (14)$$

$$D = \left(10^{\left(\frac{-1010}{T}\right) - 1.3246}\right) \times 1 \times 10^{-4} \quad (T \text{ in K}) \quad (15)$$

2.3 An independent appraisal of photo-production rates

The photochemical model of Fichot and Miller (2010) was used to calculate monthly climatologies of depth-integrated photo-production rates of OCS in the global ocean.

Briefly, the photochemical model used three components to calculate depth-resolved photochemical rates in the global ocean: (1) a radiative transfer model for the determination of cloud-corrected UV-visible (290–490 nm) downward scalar irradiance, (2) the SeaUV algorithm (Fichot et al., 2008), used to calculate the spectral diffuse attenuation coefficient of UV and CDOM absorption coefficient (290–490 nm) from satellite ocean

A new model for the global biogeochemical cycle of carbonyl sulfide

T. Launois et al.

Title Page

Abstract

Introduction

Conclusions

References

Tables

Figures



Back

Close

Full Screen / Esc

Printer-friendly Version

Interactive Discussion



annual mean chlorophyll concentrations and a stronger seasonal cycle. Observed mid and high latitude chlorophyll levels showed values three to four times larger than chlorophyll levels in tropical regions, which was also well captured with NEMO-PISCES. However, the model generally underestimated the chlorophyll concentration in the most oligotrophic subtropical zones of the global ocean.

3.2 Evaluation of the depth-distribution of a_{350} and OCS concentrations at the BATS site

In order to provide an evaluation of modeled vertical distributions of OCS concentrations, in this subsection we present vertical monthly mean profiles of a_{350} and OCS concentration from 1-D simulation runs with NEMO-PISCES for the BATS site (31° N, 64° W). Wherever possible, we compared these simulated profiles with relevant in situ measurements. In situ measurements for OCS concentrations remain scarce at this point, especially the ones evaluating the individual contribution of each of the OCS formation and destruction processes. Therefore, the cruise measurements around the BATS site from Cutter et al. (2004) are often used as a reference.

3.2.1 Vertical profiles for a_{350}

Our MODIS-Aqua based extrapolation (Eq. 6) resulted in the highest values of simulated a_{350} (up to 0.15 m^{-1} , both in January and in August), while the parameterization from Preiswerk et al. (2000) resulted in a_{350} values that were about twice as low (Fig. 5), consistent with the difference in the respective a_{350} -chlorophyll formulations (Fig. 3). Values for a_{350} deduced from Morel and Gentili (2009) (Eq. 2) gave an intermediary result. The pronounced August maximum around 80 m depth (Fig. 5b) reflected a chlorophyll content maximum at this depth (a_{350} is monotonically increasing for low levels of chlorophyll). On the contrary, low a_{350} values near the surface translated a local minimum in the chlorophyll content. Note also the quick decrease of chlorophyll concentrations, and therefore the decreasing a_{350} , for depths below 80 m in August. In

January the mixed layer was 120 m-thick in NEMO-PISCES at the BATS site (Fig. 5a). Chlorophyll content (thus a_{350}) remained important and constant over the first 120 m of the ocean before an abrupt decrease in the pycnocline. For both January and August, chlorophyll concentrations and a_{350} values became negligible below 200 m, with the exception of a_{350} calculated with the relation proposed in this work.

3.2.2 Vertical OCS concentration profiles

Differences in a_{350} estimations using the relations in Eqs. (2) to (7) led to 3-fold difference between the most extreme near-surface OCS maximum concentrations simulated by NEMO-PISCES (from 100 to 300 pmol L⁻¹ in August and from 30 to 85 pmol L⁻¹ in January). In the photic zone (the first 30 m below the surface, as implemented in NEMO-PISCES), August subsurface OCS concentrations (Fig. 5d) were clearly driven by the photo-production (vertical profile of photo-production not shown here). Where the influence of UV-light irradiance is smaller or negligible (below 30 m in August or in the entire water column in January), OCS concentration profiles are driven by the predominant dark-production (vertical profile of the dark-production contribution not shown here). Therefore, in these layers, OCS concentrations mostly followed the chlorophyll content profiles. Thus, OCS concentration profiles simulated with NEMO-PISCES in January showed a drop below the mixed layer (below 120 m), and became negligible below 200 m. In August, the highest concentrations were found at the surface. A second peak of OCS levels was found around 80 m depth, where chlorophyll content peaks. Deeper, the OCS concentrations decreased, down to negligible values below 200 m.

OCS concentrations simulated with NEMO-PISCES showed very large values in the few first meters under the surface, averaging 70, 90 or even 270 pmol L⁻¹ in August at BATS site, depending on the a_{350} -chlorophyll relation used. Some OCS levels measured with buoys during a field campaign in August 1999 at BATS peaked at 150 pmol L⁻¹ in the first 3 m (Cutter et al., 2004), showing a potential to reach such high values. The simulation using Morel and Gentili (2009) formulation for a_{350} -chlorophyll showed the best agreement with these observations.

The lower OCS concentrations in deeper layers reflected the quick removal of OCS by hydrolysis in the model (vertical profile of the hydrolysis contribution not shown here). This behavior fit well with the estimated short lifetime of the OCS molecule in marine waters, ranging between 4 and 13.4 h, according to the models of Elliot et al. (1989) and Radford-Knoery and Cutter (1993), respectively.

3.3 Spatial and seasonal variability of OCS production and removal processes

3.3.1 Surface a_{350} patterns

Absorption coefficients of CDOM at 350 nm (a_{350}) simulated using NEMO-PISCES were evaluated for the different formulations of a_{350} against the annual climatology of a_{350} derived from MODIS Aqua ocean color as in Fichot and Miller (2010). The MODIS Aqua-derived a_{350} (Fig. 6a) showed minimal values in the subtropical gyres, and maximum values in coastal regions and at high latitudes (higher than 45° N and 45° S). Note that the MODIS Aqua derived values should not be considered as direct observations but only as an independent estimate relying on a generic relation (i.e., a statistical model).

Regions where a_{350} was not accurately modeled also suffered from biases in simulated chlorophyll values. Therefore the highest a_{350} values observed near the coasts were not represented in NEMO-PISCES due to its limited spatial resolution. Additionally, the simulated chlorophyll maps (thus those of a_{350} as well) showed a higher contrast between low and high latitudes than the SeaWiFS derived observations (Fig. 4). In tropical regions (30° S–30° N), especially in the Atlantic Ocean, the Indian Ocean and in the Western Pacific Warm Pool, chlorophyll levels simulated by NEMO-PISCES were underestimated by a factor of two compared to the SeaWiFS chlorophyll observations (Fig. 4). As these are regions of warm ocean waters favorable to OCS dark-production, the consequence might be an underestimation of OCS production in these regions. Finally, NEMO-PISCES-simulated chlorophyll levels at mid and high latitudes were similar for northern and southern oceans, with average values around 0.5 mg m⁻³.

A new model for the global biogeochemical cycle of carbonyl sulfide

T. Launois et al.

Title Page

Abstract

Introduction

Conclusions

References

Tables

Figures



Back

Close

Full Screen / Esc

Printer-friendly Version

Interactive Discussion



However, chlorophyll concentrations deduced from satellite observations showed average mid and high latitude values around 0.2 mg m^{-3} in the Southern Hemisphere and 0.5 to 1 mg m^{-3} in the Northern Hemisphere. Thus, the NEMO-PISCES model overestimated the chlorophyll concentrations by a factor of 2 over most of the mid and high latitudes of the Southern Hemisphere – especially in the Pacific Ocean and south of Australia (Fig. 4). Therefore, our modeled OCS production in the Southern Hemisphere is likely overestimated.

The different a_{350} -chlorophyll relations used in the present work (Eq. (2), Eq. (3) and Eq. 6) led to simulated values of a_{350} differing by as much as a factor of three. The CDOM absorption coefficient values obtained with the formulations of Preiswerk et al. (2000) and Morel and Gentili (2009) were similar to the MODIS-derived estimates for low and mid latitudes (below 60° S and 60° N), but largely underestimated at high latitudes in the Northern Hemisphere, with values two to three times smaller than the MODIS-derived estimates (Fig. 6). Conversely, the formulation presented in this work (Eq. 6) correctly reproduced the observed levels of a_{350} in the northern high latitudes, but clearly overestimated the values for CDOM absorption coefficient at low latitudes and in the Southern Hemisphere: simulated a_{350} values in some subtropical oligotrophic regions reached values three to four times higher than the MODIS derived values.

3.3.2 Photo-production rates

In the present study, the a_{350} -dependent NEMO-PISCES model and the AQY dependent photochemical model from Fichot and Miller (2010) were used to provide two independent estimates of OCS photo-production rates. Sensitivity tests were performed on the annual global OCS photo-production over the entire water column (from the sea surface to the ocean floor). Both models were run with different formulations of a_{350} (NEMO-PISCES model) or using different AQY (Fichot and Miller photochemical model) from the literature.

A new model for the global biogeochemical cycle of carbonyl sulfide

T. Launois et al.

Title Page

Abstract

Introduction

Conclusions

References

Tables

Figures



Back

Close

Full Screen / Esc

Printer-friendly Version

Interactive Discussion



**A new model for the
global
biogeochemical cycle
of carbonyl sulfide**

T. Launois et al.

Title Page

Abstract

Introduction

Conclusions

References

Tables

Figures

◀

▶

◀

▶

Back

Close

Full Screen / Esc

Printer-friendly Version

Interactive Discussion



The AQY estimates used were collected in open ocean environments (Weiss et al., 1995a) and coastal environments (Zepp et al., 1994), respectively. Large uncertainties around AQY estimations depending on the measurement location led to large differences in the estimates of global OCS photo-production. Global OCS photo-production modeled with Fichot and Miller's model (2010) thus ranged from 876 to 5500 Gg S yr⁻¹ (Table 1). Extremely high AQY values have been measured on the continental shelf (Cutter et al., 2004), but were not considered appropriate to represent the global average ocean. Using this last value would have led to 37 700 Gg S yr⁻¹ of OCS global photo-production, far above observed photo-production levels and other model estimates.

Both the photochemical model from Fichot and Miller (2010) and the NEMO-PISCES model led to similar spatial distributions of OCS photo-production (Fig. 7). Indeed, the yearly photo-production of OCS was mostly concentrated in subtropical regions, whichever model was used. However, the highest photo-production rates were found in mid latitude regions (40–60° N and 40–60° S) during the period of maximum irradiance, as can be seen in the time-latitude diagram in Fig. 8a. Depending on the value of the driving parameter for the 2 models used (AQY or a_{350} , respectively), large uncertainties existed over the total quantities of OCS photo-produced. Global photo-production of OCS for the NEMO-PISCES model and the photochemical model from Fichot and Miller (2010) are compared in Table 1. When using the a_{350} -based model NEMO-PISCES, the range of the global OCS photo-production was reduced but still large, with estimates between 1390 and 4540 Gg S yr⁻¹, depending on which formulation was chosen to calculate a_{350} . These values were in rather good agreement with the range obtained with the AQY-based photochemical model from Fichot and Miller (2010).

The photochemical model from Fichot and Miller and NEMO-PISCES showed lower OCS photo-production rates than in situ measurements, irrespective of the a_{350} formulation. For instance, Cutter et al. (2004) estimated August photo-production rates up to 10 or 15 pmol L⁻¹ h⁻¹ in the Sargasso Sea, which is above the values of 4

to $9 \text{ pmol L}^{-1} \text{ h}^{-1}$ obtained by running the NEMO-PISCES model (with implemented Eq. (3) and Eq. (6) respectively) (Fig. 7).

3.3.3 Dark-production rates

Dark-production is a linear function of a_{350} (Eq. 8). However, temperature appears to be the main driver of global OCS dark-production as simulated by NEMO-PISCES. The time-latitude representation of dark-production rates (Fig. 8b) showed that the maximum values were located at low latitudes, in warm marine waters, despite the fact that these regions correspond to the lowest a_{350} values (Fig. 6). The dark-production rates in these regions remained relatively constant throughout the year. On the contrary, chlorophyll-rich waters at higher latitudes, leading to higher a_{350} values (Fig. 6) corresponded to colder marine waters and thus limited dark-production rates (due to the temperature dependency in Eq. 8).

Measurements from von Hobe et al. (2001) at the BATS site showed dark-production rates of 1 to $1.5 \text{ pmol L}^{-1} \text{ h}^{-1}$. NEMO-PISCES results showed a very good agreement with this data, with rates of $0.8 \text{ pmol L}^{-1} \text{ h}^{-1}$ in August at BATS (not shown). In the study of Cutter et al. (2004), calculated dark-production rates reached $4 \text{ pmol L}^{-1} \text{ h}^{-1}$ in August, significantly above the simulated range by NEMO-PISCES. Von Hobe et al. (2001) estimated that dark-production produces around 50 % of OCS at these low latitudes. In the NEMO-PISCES model, dark-production only represented 34 % of the OCS produced at low latitudes, and 66 % of OCS is photo-produced.

3.3.4 Hydrolysis rates

Figure 2 presents the hydrolysis reaction constant as a function of temperature for a given pH, as given by the Kamyshny et al. (2003) and Elliott et al. (1989) formulations. Both formulations relate the OCS hydrolysis to the OCS concentration and to the seawater pH (Eqs. 11a and 11b). At a given pH, the difference between the two formulations was leading to a 50 % difference in the hydrolysis constant for seawater

A new model for the global biogeochemical cycle of carbonyl sulfide

T. Launois et al.

Title Page

Abstract

Introduction

Conclusions

References

Tables

Figures



Back

Close

Full Screen / Esc

Printer-friendly Version

Interactive Discussion



temperatures above 12 °C (Fig. 2). A comparison between time-latitude maps of the hydrolysis rate (Fig. 8c) and the OCS concentration (in Supplement Fig. S1) suggests that OCS hydrolysis rates in NEMO-PISCES are largely driven by OCS levels. These spatio-temporal variation patterns only slightly differ around the equator, where marine waters are somewhat less alkaline, which leads to a limitation of the OCS hydrolysis rate through pH influence. Simulations run with two different hydrolysis parameterizations (based on Eq. 9a or Eq. 9b) provide global OCS emissions diverging by a factor of 2.5 (see Fig. 10).

3.3.5 Surface concentration patterns

Maps of annual mean surface OCS concentration patterns at sea surface simulated with NEMO-PISCES are presented on Fig. 9 (right column). NEMO-PISCES simulations produced maximum annual mean OCS levels in equatorial and sub-tropical regions, where dark-production was maximal and photo-production was constantly active. In low latitude marine waters, OCS concentrations remained nearly constant throughout the year (Supplement Figs. S1 and 9). However, the model showed a strong seasonal variability of OCS concentrations for mid and high latitudes, with roughly a factor 10 difference between maximal and minimal OCS concentration levels reached throughout the year. These spatial distributions and the intra-annual variation amplitudes were relatively independent of the formulation used in NEMO-PISCES to calculate a_{350} .

OCS concentrations measured near European shores and estuarine regions over the year, showed large spatial and temporal variability (Uher, 2006). Measured OCS concentrations in estuarine regions ranged between 258 pmol L⁻¹ in winter and 433 pmol L⁻¹ in summer, while more limited values were measured near shores ranging from 40 pmol L⁻¹ in winter to 100 pmol L⁻¹ in summer. Von Hobe et al. (2003) also measured summer OCS surface maximum levels reaching 120 pmol L⁻¹, in an upwelling region near the Portuguese coast. When using the MODIS-Aqua-based a_{350} formulation (Eq. 6) which gives the best representation of a_{350} in the region (Fig. 6),

A new model for the global biogeochemical cycle of carbonyl sulfide

T. Launois et al.

Title Page

Abstract

Introduction

Conclusions

References

Tables

Figures

◀

▶

◀

▶

Back

Close

Full Screen / Esc

Printer-friendly Version

Interactive Discussion

simulated OCS concentrations in estuarine regions range between 50 pmol L^{-1} in winter and 300 pmol L^{-1} in summer, while more limited values were also simulated near shores ranging from 30 pmol L^{-1} in winter to 100 pmol L^{-1} in summer (Fig. 9). NEMO-PISCES matches correctly the seasonal amplitude of OCS concentrations measured in these areas and represents quite accurately the absolute values measured near the shores in these cruises. However, as expected, the lack of resolution of the model translates into an under-estimation of the estuarine concentrations.

The formulation used to calculate a_{350} values did not affect the global spatial distribution of OCS concentrations, but it largely influenced the absolute value of the simulated OCS concentrations. For instance, maximal OCS concentrations in tropical sub-surface waters were estimated close to 300 pmol L^{-1} with the MODIS-Aqua-based a_{350} formulation (Eq. 6), while Morel and Gentili (2009) (Preiswerk et al., 2000)-based estimates only reached one half (one third, respectively) of these modeled maximal concentrations (Fig. 9). Note that the formulation of Morel and Gentili (2009) led to results that were in better agreement with the campaign measurements described in Sect. 3.2.2 (Cutter et al., 2004; von Hobe et al., 2001).

4 Discussion

The limited number of studies which have attempted to quantify OCS production and removal processes individually have yielded widely differing results. Several parameterizations for each process have been proposed and each parameterization remains poorly constrained. In this section we present our “best guess” formulations for the individual OCS-related processes in the NEMO-PISCES model.

Measurement campaigns used to determine dark-production functions are particularly scarce. The dark-production parameterization that we used is related to the CDOM absorption coefficient at 350 nm, as a parameterization of the link with organic matter content and biological activity in marine environments. However, there is no rationale

for dark-production to be dependent of colored organic matter content (CDOM, chlorophyll) since this process occurs at times when no light is available.

In a rare example of observation-based dark-production parameterization effort, von Hobe et al. (2003) used an experimental setup that allows them to equate the OCS dark-production rate to the hydrolysis rate, and thus expressed the first as a function of a measurement of the latter. In their estimate of the hydrolysis rate, von Hobe et al. (2003) use the Elliott et al. (1989) formulation for the OCS hydrolysis constant. Thus, our use of the von Hobe et al. (2003) dark-production parameterization is consistent with the choice of the Elliott et al. (1989) parameterization for OCS hydrolysis.

As previously described, simulated a_{350} values can be far from the observed values in warm water regions depending on the a_{350} formulation used (Fig. 6). This potentially leads to the largest errors in the dark-production rate estimates. In this context, we have found the Morel and Gentili (2009) a_{350} parameterization to perform best when evaluated against a_{350} values derived from MODIS-Aqua data at low latitudes, as well as at high latitudes in the Southern Hemisphere (Sect. 3.3.1). This formulation may, however, lead to an underestimation of a_{350} at high latitudes in Northern Hemisphere.

We have chosen the Uher et al. (1997) formulation for photoproduction associated with the Morel and Gentili parameterization for a_{350} (Eq. 2) and the Elliott formulation for the hydrolysis constant as the standard parameterizations for OCS processes in NEMO-PISCES, based on the arguments above. Time-latitude diagrams for photo- and dark-production, hydrolysis and surface OCS fluxes using these parameterizations are represented in Fig. 8. The time-latitude diagram representing the surface layer OCS concentration with the same settings is shown in Supplement Fig. S1.

The standard run of NEMO-PISCES suggests most OCS is produced photochemically. Even at low latitudes, where warm water regions favor dark-production of OCS, photo-production represents 66% of OCS production pathway (Fig. 8). In this simulation, low latitudes are the only regions where dark-production rates compensate for hydrolysis removal of OCS. The highest annual mean OCS concentrations modeled using best guess parameterizations range between 100 and 200 pmolL⁻¹ and

A new model for the global biogeochemical cycle of carbonyl sulfide

T. Launois et al.

Title Page

Abstract

Introduction

Conclusions

References

Tables

Figures

◀

▶

◀

▶

Back

Close

Full Screen / Esc

Printer-friendly Version

Interactive Discussion



A new model for the global biogeochemical cycle of carbonyl sulfide

T. Launois et al.

Title Page

Abstract

Introduction

Conclusions

References

Tables

Figures

◀

▶

◀

▶

Back

Close

Full Screen / Esc

Printer-friendly Version

Interactive Discussion



are encountered around the equator, especially in Central and Eastern Pacific Ocean. At mid and high latitudes, simulated annual mean OCS concentrations are included between 10 and 60 pmol L⁻¹. These regions show higher seasonal amplitude in OCS concentrations, especially around 60° N and 40° S, where periods of irradiance maxima (resp. minima) lead to simulated OCS concentrations of 150 pmol L⁻¹ (resp. 10 pmol L⁻¹). In these regions, simulated levels are largely consistent with in situ measurements from Cutter et al. (2004) and von Hobe et al. (2003).

Surface OCS concentrations simulated by NEMO-PISCES are the main driver of the model's sea–air OCS fluxes (Figs. 8d and S1 in the Supplement). The regions with the highest sea surface OCS concentrations (tropics and mid latitudes during maximal irradiance seasons) are the regions emitting the largest quantities of OCS. Multiple measurement campaigns (Rasmussen et al., 1982; Ferek and Andreae, 1983; Uher, 2006) have shown that coastal environments can have OCS concentrations 5 to 10 times higher than those measured at the surface of open ocean waters in oligotrophic regions. As shown in Fig. 6, MODIS-derived a_{350} reach maximal values along shores but the NEMO-PISCES model does not represent these localized maxima due to the poor model resolution in these regions. These narrow areas have an important potential in OCS production and show under-estimated OCS concentrations in NEMO-PISCES.

Air–sea exchange of OCS is also enhanced by warm surface waters and strong winds (Eq. 12). Both variables have a noticeable impact on the simulated OCS surface fluxes, especially at low latitudes. In fact, NEMO-PISCES simulations show the highest OCS emissions around the equator even if some mid and high latitude oceanic regions show higher OCS sea surface concentrations for some periods of the year: OCS outgassing rates in July along the Equator are twice as important as outgassing taking place in Northern mid latitudes in the same period (Fig. 8d), despite the mid latitudes showing surface OCS concentrations 60 % higher than those simulated around the Equator.

We have investigated the sensitivity of the sea–air fluxes to the parameterizations of OCS production and removal processes. Global and regional annual sea–air OCS

fluxes obtained in these tests are summarized in Fig. 10. Simulated fluxes by Kettle et al. (2002) are also represented on the Fig. 10 (black line) for comparison. While the different parameterization choices lead to a large spread in the simulated OCS fluxes towards the atmosphere, NEMO-PISCES consistently produces higher estimates of the global sea–air OCS fluxes than the ones previously estimated by Kettle et al. (2002). Total emitted OCS simulated using the “best guess” parameterization of NEMO-PISCES reaches 813 Gg S yr^{-1} , far above the modeled direct source of 40 Gg S yr^{-1} from Kettle et al. (2002) and consistent with the revised global oceanic flux based on atmospheric measurements and a model for leaf uptake, proposed by Berry et al. (736 Gg S yr^{-1}). Extrapolations of measurements carried out in the Mediterranean sea and the Indian ocean by Mihalopoulos et al. (1992) led to an independent estimate of 213 Gg S yr^{-1} , markedly lower than the mean annual global flux simulated with NEMO-PISCES. Kettle et al. (2002) described the global direct exchange of OCS between the ocean and the atmosphere as highly uncertain, and pointed out the fact that in some of their simulations, some regions of the ocean behaved like sinks of atmospheric OCS at certain periods of the year. Some regions at extreme high latitudes also act like a sink of atmospheric OCS in NEMO-PISCES for certain periods of the year (Fig. 8d).

- The different parameterizations available for the different processes presented in this paper lead to different global flux estimates, ranging from 573 Gg S yr^{-1} (when using the CDOM absorption coefficient values obtained with the formulations of Preiswerk et al. (2000) and the higher values of the Elliot-based hydrolysis constant) to $3997 \text{ Gg S yr}^{-1}$ (when using the MODIS-derived a_{350} and the lower values of the Kamyshny-based hydrolysis constant). Our “best-guess” parameterization of NEMO-PISCES shows the best agreement with the in situ evaluation of the individual processes, and stands in the lower part of the range of OCS direct annual emissions by ocean at a global scale.

A new model for the global biogeochemical cycle of carbonyl sulfide

T. Launois et al.

[Title Page](#)[Abstract](#)[Introduction](#)[Conclusions](#)[References](#)[Tables](#)[Figures](#)[Back](#)[Close](#)[Full Screen / Esc](#)[Printer-friendly Version](#)[Interactive Discussion](#)

A new model for the global biogeochemical cycle of carbonyl sulfide

T. Launois et al.

Title Page

Abstract

Introduction

Conclusions

References

Tables

Figures



Back

Close

Full Screen / Esc

Printer-friendly Version

Interactive Discussion



– Changing the parameterization also changes the seasonal amplitude of the simulated OCS flux by up to a factor five for Northern and Southern Hemisphere oceans but no significant change is noticeable on the seasonal amplitude of OCS fluxes in the tropical region.

5 Recent efforts to constrain global OCS fluxes have led to a growing number of measurements and consequent revisions of soil and vegetation uptake estimates. Multiple recent studies have suggested that soil and vegetation uptakes were underestimated in the new assessments of the global OCS cycle and have suggested a global sink for both of up to $1000 \text{ Gg S yr}^{-1}$, much larger than the initial estimates of approximately 300 Gg S yr^{-1} (Berry et al., 2013; Suntharalingam et al., 2008). Knowing that atmospheric OCS levels show no trend over the last two decades (Montzka et al., 2007), the global cycle of OCS is expected to be balanced on a global scale. In order to compensate re-estimated sinks based on a mechanistic description of leaf OCS uptake (using SIB3 land surface model), Berry et al. (2013) have suggested that the ocean provides the missing source. Using a simple inversion approach to optimize the oceanic missing source, given known land natural and anthropogenic fluxes, the authors evaluated that the ocean should emit 736 Gg S yr^{-1} . Moreover, the best-fit optimization used by the authors revealed that the missing source should be concentrated over the low latitudes in order to best fit the atmospheric data recorded at NOAA stations.

20 Using our “best guess” parameterization for NEMO-PISCES leads to relatively constant global OCS outgassing throughout the year, with a seasonal amplitude of only 10 %. Tropical regions (30° S – 30° N) emit the major part of the OCS, and represent up to 45 % of the total emitted OCS towards the atmosphere. Tropical exchanges show almost no variation throughout the year. Northern and southern oceanic regions at mid and high latitudes (higher than 30° N and 30° S , respectively) participate to 20 % and 35 %, respectively, of the OCS global flux towards atmosphere each year (Supplement Fig. S2).

Despite the consistency in terms of global OCS fluxes quantities and spatial distribution between best guess parameterizations of NEMO-PISCES and indirect oceanic

A new model for the global biogeochemical cycle of carbonyl sulfide

T. Launois et al.

Title Page

Abstract

Introduction

Conclusions

References

Tables

Figures



Back

Close

Full Screen / Esc

Printer-friendly Version

Interactive Discussion



source estimate from Berry et al. (2013), the simulated outgassing using NEMO-PISCES show a large envelope when using the different possible parameterizations. Most of them lead to much larger global flux estimates than previous studies, ranging between 573 and 3997 Gg S yr⁻¹. Higher estimates for OCS fluxes with NEMO-PISCES result from using hydrolysis constant from Kamyshny et al. (2003) or a_{350} calculation proposed in this present work. Kamyshny-based hydrolysis constant is not consistent with the Elliot-based hydrolysis constant used to determinate OCS dark-production implemented in NEMO-PISCES. Moreover, calculation of a_{350} proposed in this work was demonstrated to lead to large over-estimations of the a_{350} values compared with the observational data. Both parameterizations lead to very large estimates of OCS fluxes towards the atmosphere, which are not likely since they would lead to highly unbalanced atmospheric OCS budget.

5 Conclusion

At a global scale, the ocean is supposed to be the largest direct and indirect source of OCS to the atmosphere. Recent studies (Suntharalingham et al., 2008; Berry et al., 2013) pointed out the need to re-evaluate the global OCS sinks, signaling a possible underestimation in previous assessments. There is currently no trend in the atmospheric levels of OCS (Montzka et al., 2007), thus increased sinks have to be compensated by a source, currently missing from the global OCS budget. The recent inversion study of Berry et al. (2013) and previous Atmospheric Chemistry Experiment ACE observational analysis of Barkley et al. (2008) have suggested that a large part of this missing source should be ocean outgassing at low latitudes.

Previous studies of the OCS production and removal processes in the ocean have only led to poor constraint of the potential global sea–air fluxes. Moreover, numerical simulations have led to relatively small modeled global fluxes of OCS outgassed to the atmosphere. In this study we have selected different parameterizations for the most

A new model for the global biogeochemical cycle of carbonyl sulfide

T. Launois et al.

Title Page

Abstract

Introduction

Conclusions

References

Tables

Figures



Back

Close

Full Screen / Esc

Printer-friendly Version

Interactive Discussion



important OCS production and removal processes, which we then implemented in the 3-D NEMO-PISCES ocean model.

5 Simulated fluxes with this model showed a potential for large global OCS fluxes, with our best guess simulation reaching a net emission of OCS up to 800 Gg S yr^{-1} , much larger than previous estimated ranges. Moreover, the resulting spatial distribution of these fluxes supports the assumed key role of tropical regions, where warm marine waters can produce high levels of OCS with little organic matter. Our modeled ocean-atmosphere OCS fluxes were concentrated in the equatorial and subtropical regions, which accounted for half of the global OCS outgassing to the atmosphere. This result
10 is in good agreement with the necessary distribution of the missing oceanic source of OCS that would be consistent with the atmospheric OCS concentration gradients (north south gradient for instance), measured at the different stations of the NOAA network. The uncertainties around OCS fluxes, however, will remain very large until a wide array of measurements focusing on the individual processes is available, to accurately calibrate the relative importance of each marine OCS production and removal process.
15

The Supplement related to this article is available online at doi:10.5194/acpd-14-20677-2014-supplement.

Author contribution. S. Belviso and P. Peylin designed the experiments. T. Launois did the bibliography research for process parameterizations and developed the NEMO-PISCES specific
20 OCS module code and performed the simulations with the help from L. Bopp. C. Fichot run tests with the SeaUV model that he developed, allowing comparison of OCS photo-production rates with the results obtained with NEMO-PISCES. T. Launois prepared the manuscript with contributions from all co-authors.

Acknowledgements. The authors wish to thank E. Campbell who shared simulation results from Kettle et al. (2002) and allowed the comparisons done in this work. We also thank
25 A. Gainusa-Bogdan for improving the manuscript.

References

- Aumont, O. and Bopp, L.: Globalizing results from ocean in situ iron fertilization studies, *Global Biogeochem. Cy.*, 20, GB2017, doi:10.1029/2005GB002591, 2006.
- Barkley, M. P., Palmer, P. I., Boone, C. D., Bernath, P. F., and Suntharalingam, P.: Global distributions of carbonyl sulfide in the upper troposphere and stratosphere, *Geophys. Res. Lett.*, 35, L14810, doi:10.1029/2008GL034270, 2008.
- Berry, J., Wolf, A., Campbell, J. E., Baker, I., Blake, N., Blake, D., and Zhu, Z.: A coupled model of the global cycles of carbonyl sulfide and CO₂: a possible new window on the carbon cycle, *J. Geophys. Res.-Biogeo.*, 118, 842–852, 2013.
- Bopp, L., Aumont, O., Belviso, S., and Blain, S.: Modelling the effect of iron fertilization on dimethylsulphide emissions in the Southern Ocean, *Deep-Sea Res. Pt. II*, 55, 901–912, 2008.
- Bricaud, A., Babin, M., Morel, A., and Claustre, H.: Variability in the chlorophyll-specific absorption coefficients of natural phytoplankton: analysis and parameterization, *J. Geophys. Res.-Oceans*, 100, 13321–13332, 1995.
- Brühl, C., Lelieveld, J., Crutzen, P. J., and Tost, H.: The role of carbonyl sulphide as a source of stratospheric sulphate aerosol and its impact on climate, *Atmos. Chem. Phys.*, 12, 1239–1253, doi:10.5194/acp-12-1239-2012, 2012.
- Campbell, J. E., Carmichael, G. R., Chai, T., Mena-Carrasco, M., Tang, Y., Blake, D. R., and Stanier, C. O.: Photosynthetic control of atmospheric carbonyl sulfide during the growing season, *Science*, 322, 1085–1088, 2008.
- Chin, M. and Davis, D. D.: A reanalysis of carbonyl sulfide as a source of stratospheric background sulfur aerosol, *J. Geophys. Res.-Oc. Atmos.*, 100, 8993–9005, 1993.
- Chin, M., Rood, R. B., Lin, S. J., Müller J. F., and Thompson, A. M.: Atmospheric sulfur cycle simulated in the global model GOCART: model description and global properties, *J. Geophys. Res.-Oc. Atmos.*, 105, 24671–24687, 2000.
- Cutter, G. A., Cutter, L. S., and Filippino, K. C.: Sources and cycling of carbonyl sulfide in the Sargasso Sea, *Limnol. Oceanogr.*, 49, 555–565, 2004.
- Elliott, S., Lu, E., and Rowland, F. S.: Rates and mechanisms for the hydrolysis of carbonyl sulfide in natural waters, *Environ. Sci. Technol.*, 23, 458–461, 1989.
- Ferek, R. J. and Andreae, M. O.: Photochemical production of carbonyl sulphide in marine surface waters, *Global Biogeochem. Cy.*, 6, 175–183, 1984.

A new model for the global biogeochemical cycle of carbonyl sulfide

T. Launois et al.

Title Page

Abstract

Introduction

Conclusions

References

Tables

Figures



Back

Close

Full Screen / Esc

Printer-friendly Version

Interactive Discussion



A new model for the global biogeochemical cycle of carbonyl sulfide

T. Launois et al.

Title Page

Abstract

Introduction

Conclusions

References

Tables

Figures



Back

Close

Full Screen / Esc

Printer-friendly Version

Interactive Discussion



Fichot, C. G. and Miller, W. L.: An approach to quantify depth-resolved marine photochemical fluxes using remote sensing: application to carbon monoxide (CO) photoproduction, *Remote Sens. Environ.*, 114, 1363–1377, 2010.

Fichot, C. G., Sathyendranath, S., and Miller, W. L.: SeaUV and SeaUVC: algorithms for the retrieval of UV/Visible diffuse attenuation coefficients from ocean color, *Remote Sens. Environ.*, 112, 1584–1602, 2008.

Flöck O. R., Andreae, M. O., and Dräger M.: Environmentally relevant precursors of carbonyl sulfide in aquatic systems, *Mar. Chem.*, 59, 71–85, 1997.

Johnson, J. E. and Harrison, H.: Carbonyl sulfide concentrations in the surface waters and above the Pacific Ocean, *J. Geophys. Res.-Oc. Atmos.*, 91, 7883–7888, 1986.

Kamysnyh, A., Goifman, A., Rizkov, D., and Lev, O.: Formation of carbonyl sulfide by the reaction of carbon monoxide and inorganic polysulfides, *Environ. Sci. Technol.*, 37, 1865–1872, 2003.

Kettle, A. J., Kuhn, U., von Hobe, M., Kesselmeier, J., and Andreae, M. O.: Global budget of atmospheric carbonyl sulfide: Temporal and spatial variations of the dominant sources and sinks, *J Geophys Res-Atmos*, 107, 4658, doi:10.1029/2002JD002187, 2002.

Kloster, S., Feichter, J., Maier-Reimer, E., Six, K. D., Stier, P., and Wetzell, P.: DMS cycle in the marine ocean-atmosphere system – a global model study, *Biogeosciences*, 3, 29–51, doi:10.5194/bg-3-29-2006, 2006.

Koch, D., Jacob, D., Tegen, I., Rind, D., and Chin, M.: Tropospheric sulfur simulation and sulfate direct radiative forcing in the Goddard Institute for Space Studies general circulation model, *J. Geophys. Res.-Oc. Atmos.*, 104, 23799–23822, 1999.

Large, W. G. and Yeager, S. G.: The global climatology of an interannually varying air–sea flux data set, *Clim. Dynam.*, 33, 341–364, 2008.

Madec, G.: NEMO Ocean General Circulation Model Reference Manuel, Internal Report, LODYC/IPSL, Paris, 2008.

Mihalopoulos, N., Nguyen, B. C., Putaud, J. P., and Belviso, S.: The oceanic source of carbonyl sulfide (COS), *Atmos. Environ.*, 26, 1383–1394, 1992.

Morel, A.: Optical modeling of the upper ocean in relation to its biogenous matter content (case I waters), *J. Geophys. Res.-Oceans*, 93, 10749–10768, 1988.

Morel, A. and Gentili, B.: A simple band ratio technique to quantify the colored dissolved and detrital organic material from ocean color remotely sensed data, *Remote Sens. Environ.*, 113, 998–1011, 2009.

A new model for the global biogeochemical cycle of carbonyl sulfide

T. Launois et al.

Title Page

Abstract

Introduction

Conclusions

References

Tables

Figures

◀

▶

◀

▶

Back

Close

Full Screen / Esc

Printer-friendly Version

Interactive Discussion

- Montzka, S. A., Calvert, P., Hall, B. D., Elkins, J. W., Conway, T. J., Tans, P. P., and Sweeney, C.: On the global distribution, seasonality, and budget of atmospheric carbonyl sulfide (COS) and some similarities to CO₂, *J. Geophys. Res.-Oc. Atmos.*, 112, 1984–2012, 2007.
- Notholt, J., Weisenstein, D., Kuang, Z., Rinsland, C. P., Toon, G. C., Rex, M., and Schrems, O.: Composition of the Upper Tropical Troposphere and Its Influence on the Stratospheric Aerosol Formation, EGS-AGU-EUG Joint Assembly, vol. 1, 4024 pp., 2003.
- Para, J., Coble, P. G., Charrière, B., Tedetti, M., Fontana, C., and Sempéré, R.: Fluorescence and absorption properties of chromophoric dissolved organic matter (CDOM) in coastal surface waters of the northwestern Mediterranean Sea, influence of the Rhône River, *Biogeosciences*, 7, 4083–4103, doi:10.5194/bg-7-4083-2010, 2010.
- Preiswerk, D. and Najjar, R. G.: A global, open-ocean model of carbonyl sulfide and its air–sea flux, *Global Biogeochem. Cy.*, 14, 585–598, 2000.
- Radford-Knoery, J. and Cutter, G. A.: Determination of carbonyl sulfide and hydrogen sulfide species in natural waters using specialized collection procedures and gas chromatography with flame photometric detection, *Anal. Chem.*, 65, 976–982, 1993.
- Rasmussen, R. A., Khalil, M. A. K., and Hoyt, S. D.: The oceanic source of carbonyl sulfide (OCS), *Atmos. Environ.*, 16, 1591–1594, 1982.
- Suntharalingam, P., Kettle, A. J., Montzka, S. M., and Jacob, D. J.: Global 3-D model analysis of the seasonal cycle of atmospheric carbonyl sulfide: implications for terrestrial vegetation uptake, *Geophys. Res. Lett.*, 35, L19801, doi:10.1029/2008GL034332, 2008.
- Tedetti, M. and Sempéré, R.: Penetration of ultraviolet radiation in the marine environment, a review, *Photochem. Photobiol.*, 82, 389–397, 2006.
- Uher, G.: Distribution and air–sea exchange of reduced sulphur gases in European coastal waters, *Estuar. Coast Shelf S.*, 70, 338–360, 2006.
- Uher, G. and Andreae, M. O.: Photochemical production of carbonyl sulfide in North Sea water: a process study, *Limnol. Oceanogr.*, 42, 432–442, 1997.
- Ulshöfer, V. S., Uher, G., and Andreae, M. O.: Evidence for a winter sink of atmospheric carbonyl sulfide in the northeast Atlantic Ocean, *Geophys. Res. Lett.*, 22, 2601–2604, 1995.
- Ulshöfer, V. S., Flock, O. R., Uher, G., and Andreae, M. O.: Photochemical production and air–sea exchange of carbonyl sulfide in the eastern Mediterranean Sea, *Mar. Chem.*, 53, 25–39, 1996.
- von Hobe, M., Cutter, G. A., Kettle, A. J., and Andreae, M. O.: Dark production: a significant source of oceanic COS, *J. Geophys. Res.-Oceans*, 106, 31217–31226, 2001.

**A new model for the
global
biogeochemical cycle
of carbonyl sulfide**

T. Launois et al.

Title Page

Abstract

Introduction

Conclusions

References

Tables

Figures



Back

Close

Full Screen / Esc

Printer-friendly Version

Interactive Discussion



von Hobe, M., Najjar, R. G., Kettle, A. J., and Andreae, M. O.: Photochemical and physical modeling of carbonyl sulfide in the ocean, *J. Geophys. Res.-Oceans*, 108, doi:10.1029/2000JC000712, 2003.

Wanninkhof, R.: Relationship between wind speed and gas exchange over the ocean, *J. Geophys. Res.-Oceans*, 97, 7373–7382, 1992.

Watts, S. F.: The mass budgets of carbonyl sulfide, dimethyl sulfide, carbon disulfide and hydrogen sulfide, *Atmos. Environ.*, 34, 761–779, 2000.

Weiss, P. S., Johnson, J. E., Gammon, R. H., and Bates, T. S.: Reevaluation of the open ocean source of carbonyl sulfide to the atmosphere, *J. Geophys. Res.-Oc. Atmos.*, 100, 23083–23092, 1995a.

Weiss, P. S., Andrews, S. S., Johnson, J. E., and Zafiriou, O. C.: Photoproduction of carbonyl sulfide in South Pacific Ocean waters as a function of irradiation wavelength, *Geophys. Res. Lett.*, 22, 215–218, 1995b.

Wohlfahrt, G., Brilli, F., Hörtnagl, L., Xu, X., Bingemer, H., Hansel, A., and Loreto, F.: Carbonyl sulfide (COS) as a tracer for canopy photosynthesis, transpiration and stomatal conductance: potential and limitations, *Plant Cell Environ.*, 35, 657–667, 2012.

Xu, X., Bingemer, H. G., Georgii, H. W., Schmidt, U., and Bartell, U.: Measurements of carbonyl sulfide (COS) in surface seawater and marine air, and estimates of the air–sea flux from observations during two Atlantic cruises, *J. Geophys. Res.-Oc. Atmos.*, 106, 3491–3502, 2001.

Zepp, R. G. and Andreae, M. O.: Factors affecting the photochemical production of carbonyl sulfide in seawater, *Geophys. Res. Lett.*, 21, 2813–2816, 1994.

A new model for the global biogeochemical cycle of carbonyl sulfide

T. Launois et al.

Title Page

Abstract

Introduction

Conclusions

References

Tables

Figures



Back

Close

Full Screen / Esc

Printer-friendly Version

Interactive Discussion



Table 1. Annual global photo-production of OCS in the entire water column simulated with the NEMO-PISCES model (using the three different a_{350} formulations presented in this paper) or with the photochemical model derived from Fichot and Miller (2010) (FM in the table) (using two different apparent quantum yields estimates). F: a_{350} parameterization assembled in this work; MG: a_{350} parameterization presented in Morel and Gentili (2009); P: a_{350} parameterization presented in Preiswerk et al. (2000).

Parameterization used in the runs	Total photo-produced OCS in the entire water column (Gg S yr^{-1})
NEMO-PISCES + F	4540
NEMO-PISCES + MG	1910
NEMO-PISCES + P	1390
FM + AQY from Weiss et al. (1995a)	876
FM + AQY from Zepp et al. (1994)	5500

A new model for the global biogeochemical cycle of carbonyl sulfide

T. Launois et al.

Title Page

Abstract

Introduction

Conclusions

References

Tables

Figures



Back

Close

Full Screen / Esc

Printer-friendly Version

Interactive Discussion



Table 2. Yearly global OCS flux emitted from ocean to the atmosphere (in Gg S yr^{-1}) depending on the different parameterizations presented in previous work and in this work. F: a_{350} parameterization presented in this work; MG: a_{350} parameterization presented in Morel and Gentili (2009); P: a_{350} parameterization presented in Preiswerk et al. (2000).

Study	Method	Annual flux (Gg S yr^{-1})
Chin and Davis (1993)	Interpolation of observations	200 to 900
	sea surface OCS supersaturation ratios ^a	
Watts (2000)	OCS surface concentration ^b	300 ^e
	Forward modeling	
Kettle et al. (2002) ^c	AQY/ a_{350}	hydrolysis constant
	AQY	Elliott et al. (1989)
Berry et al. (2013) ^d	from Kettle et al. (2002)	from Kettle et al. (2002)
This work standard run	a_{350} from MG	Elliott et al. (1989)
		40 ^f
		736
		813

^a Sea surface OCS supersaturation ratios from open oceans, upwelling zones and coastal regions.

^b OCS surface concentration from estuarine, coastal and open ocean environments.

^c Based on UV irradiance and apparent quantum yields from the literature. Lowest and highest boundaries of the estimates correspond to the lowest and highest AQY used.

^d 136 Gg S yr^{-1} taken from Kettle upper estimate. Added source of 600 Gg S yr^{-1} necessary to equilibrate the global budget.

^e 100 Gg S yr^{-1} from open ocean and 200 Gg S yr^{-1} from coastal shores.

^f Uncertainty range: between $-110 \text{ Gg S yr}^{-1}$ + 190 Gg S yr^{-1} .

A new model for the global biogeochemical cycle of carbonyl sulfide

T. Launois et al.

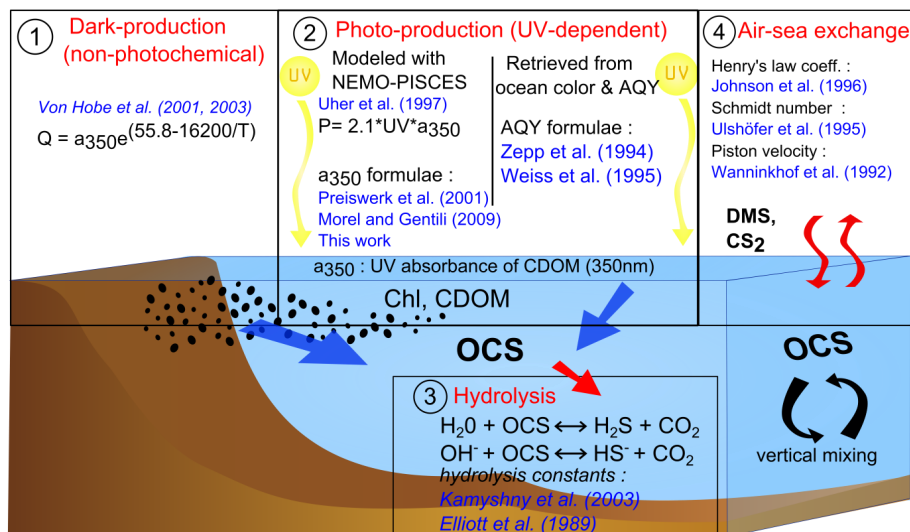


Figure 1. Main production and removal processes implemented in the NEMO-PISCES OGCM to simulate the marine OCS cycle: dark-production, photo-production and hydrolysis. Of central importance is the UV absorption coefficient at 350 nm of chromophoric dissolved organic matter (CDOM) which is derived from modeled Chl concentrations using three different relationships linking a_{350} to Chl. The simulated photo-production rates of OCS were evaluated independently using the model of Fichot and Miller (2010) and published apparent quantum yields (AQY). Aqueous OCS is removed by hydrolysis (two different formulations of the hydrolysis rate are used), lost or absorbed at the air–sea interface and mixed both vertically and horizontally. Studies relevant for sensitivity tests and model parameterization presented in this paper are displayed in blue. Oceans also emit DMS and CS₂ which are later oxidized in OCS in the atmosphere. These indirect sources of OCS are not detailed in the present study.

A new model for the global biogeochemical cycle of carbonyl sulfide

T. Launois et al.

Title Page

Abstract

Introduction

Conclusions

References

Tables

Figures

◀

▶

◀

▶

Back

Close

Full Screen / Esc

Printer-friendly Version

Interactive Discussion

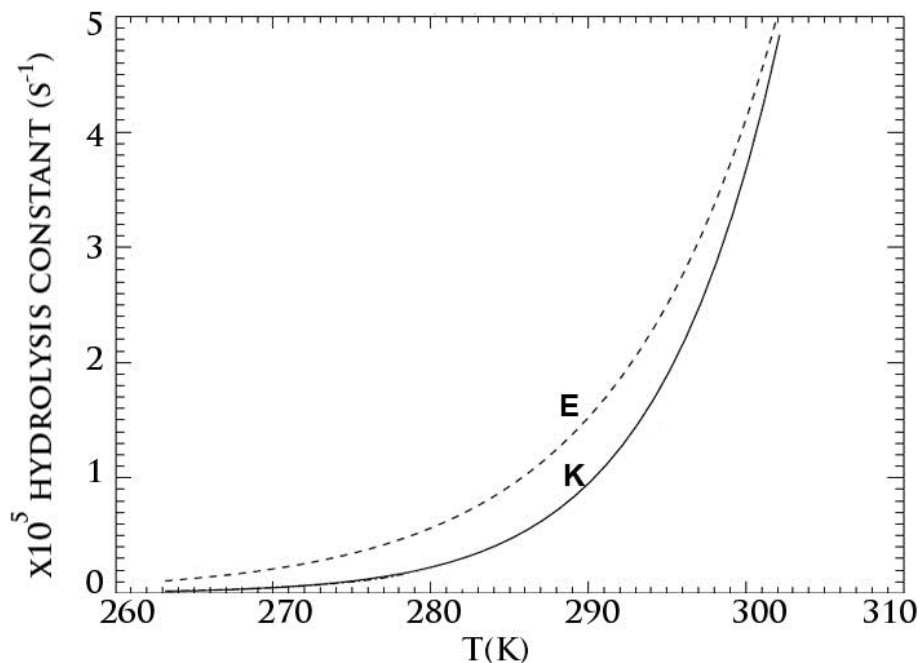


Figure 2. Temperature dependence of hydrolysis rates implemented in NEMO-PISCES. The relationships are represented for pH = 8.2, and taken from Elliott et al. (1989) (E, dashed line) or Kamyshtny et al. (2003) (K, solid line).

A new model for the global biogeochemical cycle of carbonyl sulfide

T. Launois et al.

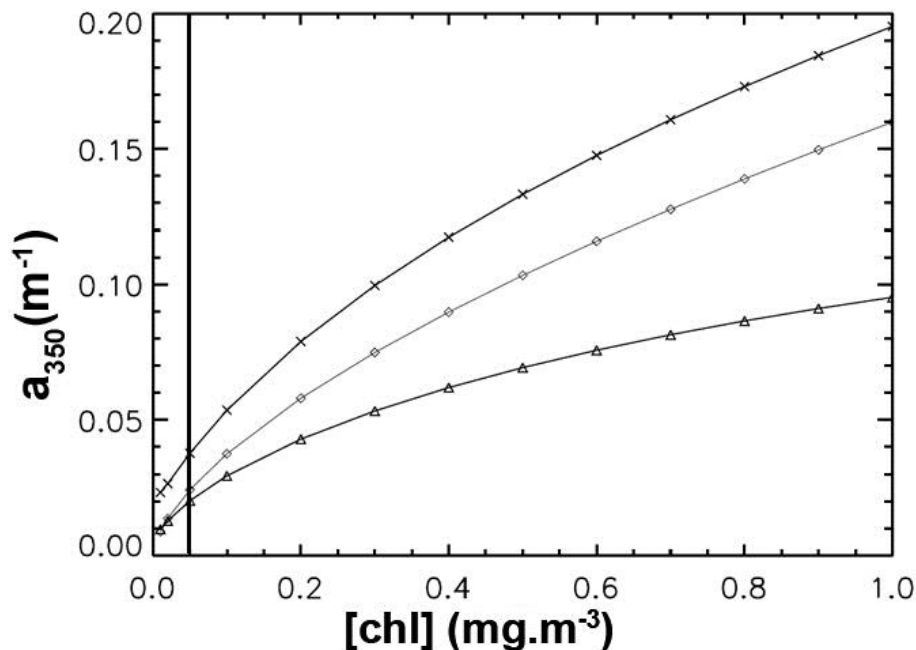


Figure 3. Relationships implemented in the NEMO-PISCES model between UV absorption coefficients for CDOM at 350 nm and chlorophyll concentrations. The 3 respective relationships are from Morel and Gentili (2009) (diamonds), Preiswerk et al. (2000) (triangles) or issued from this study, based on MODIS-Aqua ocean color (crosses). Chlorophyll concentrations in NEMO-PISCES have a fixed minimal value of 0.05 mg m^{-3} (thick vertical line).

[Title Page](#)[Abstract](#)[Introduction](#)[Conclusions](#)[References](#)[Tables](#)[Figures](#)[◀](#)[▶](#)[◀](#)[▶](#)[Back](#)[Close](#)[Full Screen / Esc](#)[Printer-friendly Version](#)[Interactive Discussion](#)

A new model for the global biogeochemical cycle of carbonyl sulfide

T. Launois et al.

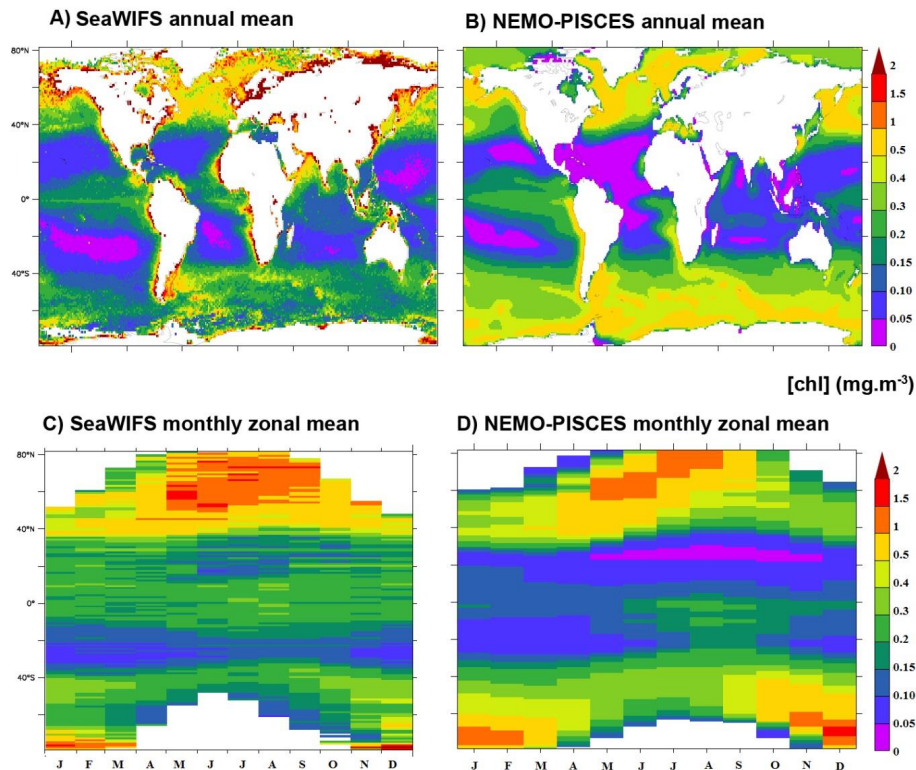


Figure 4. Comparison of remotely sensed observations of chlorophyll (left panels) with simulations performed using the NEMO-PISCES model (right panels). Top panels (**a**, **b**) represent maps of annual mean chlorophyll concentration ($\text{mg}\cdot\text{m}^{-3}$). Bottom panels (**c**, **d**) represent latitude-time maps of chlorophyll.

A new model for the global biogeochemical cycle of carbonyl sulfide

T. Launois et al.

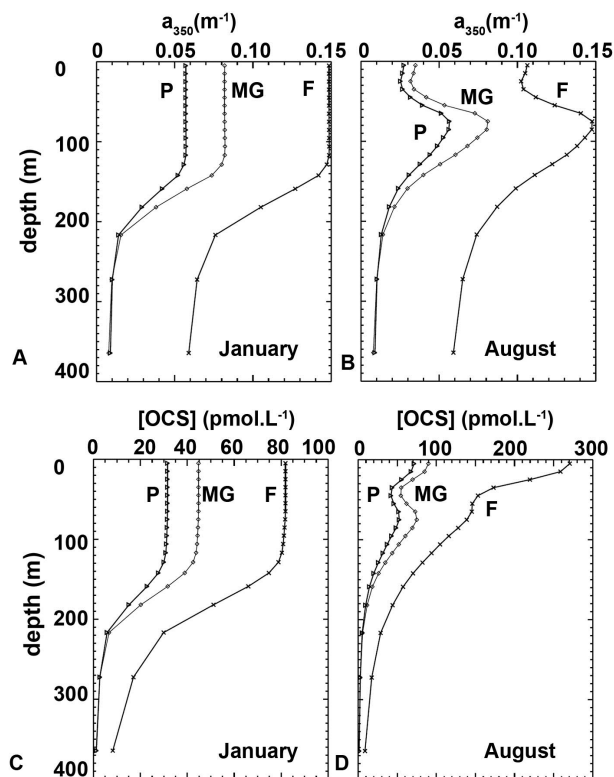


Figure 5. Monthly mean vertical profiles of a_{350} (top row) and OCS concentration (bottom row) in January (left column) and August (right column) simulated by NEMO-PISCES in a 1-D run at the Bermuda Atlantic Time Series (BATS) site. The different a_{350} profile are calculated using the formulations of Morel and Gentili (2009) (MG, diamonds), Preiswerk et al. (2000) (P, triangles) or based on MODIS-aqua data (F, black line). Symbols used on OCS concentration profile on bottom row indicate which a_{350} -chlorophyll relation was used in the simulation.

Title Page

Abstract

Introduction

Conclusions

References

Tables

Figures

◀

▶

◀

▶

Back

Close

Full Screen / Esc

Printer-friendly Version

Interactive Discussion



A new model for the global biogeochemical cycle of carbonyl sulfide

T. Launois et al.

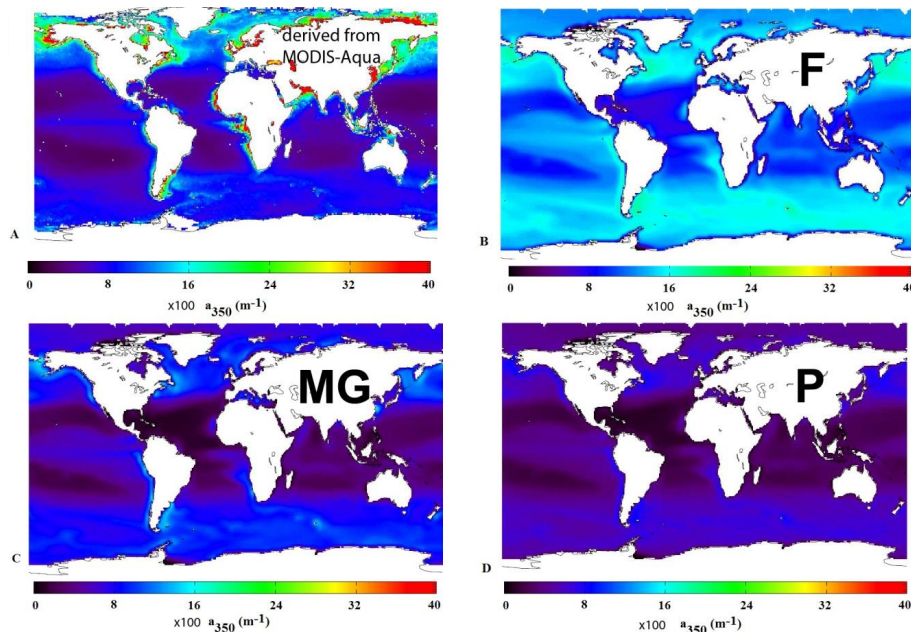


Figure 6. Comparison between annual mean surface absorption coefficient of CDOM at 350 nm: **(A)** retrieved from MODIS-Aqua satellites data, using SeaUV model (Fichot et al., 2008) and a_{320}/K_{d320} ratio from Fichot and Miller (2010) and a_{350} maps simulated with the NEMO-PISCES model using the relation described in Morel and Gentili (2009) (MG, **C**), Preiswerk et al. (2000) (P, **D**) or proposed in this work (F, **B**).

Title Page

Abstract

Introduction

Conclusions

References

Tables

Figures

◀

▶

◀

▶

Back

Close

Full Screen / Esc

Printer-friendly Version

Interactive Discussion



A new model for the global biogeochemical cycle of carbonyl sulfide

T. Launois et al.

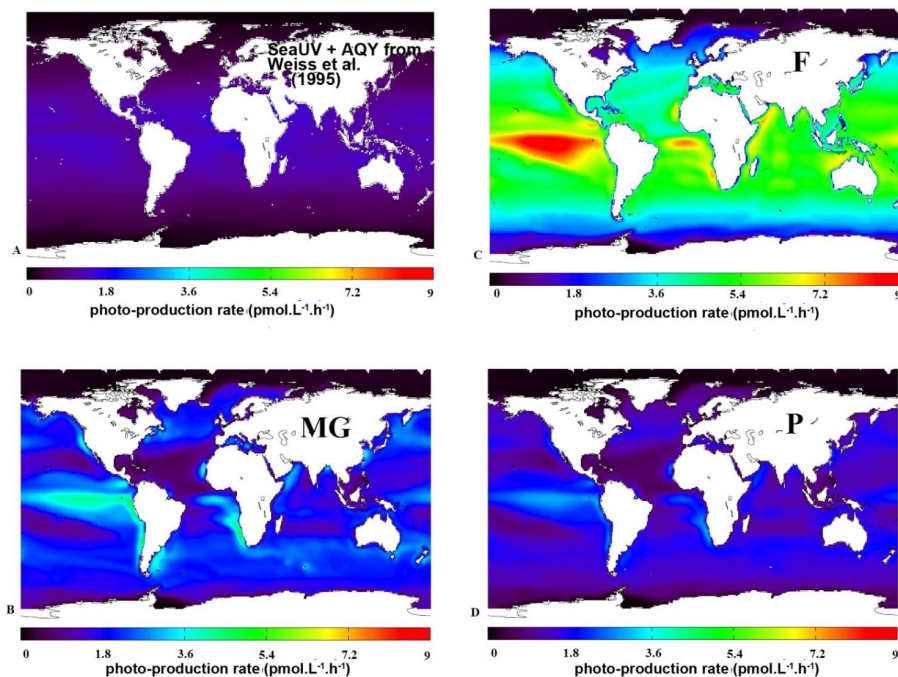


Figure 7. Annual mean photo-production rates integrated over the entire water column simulated with the photochemical model of Fichot and Miller (2010) and using the apparent quantum yield of Weiss et al. (1995a) **(A)**. Comparison with annual mean photo-production rates integrated over the entire water column simulated with the NEMO-PISCES model using a_{350} formulations from Morel and Gentili (2009) **(C)**, Preiswerk et al. (2000) **(D)** or proposed in this study **(B)**.

Title Page

Abstract

Introduction

Conclusions

References

Tables

Figures

◀

▶

◀

▶

Back

Close

Full Screen / Esc

Printer-friendly Version

Interactive Discussion



A new model for the global biogeochemical cycle of carbonyl sulfide

T. Launois et al.

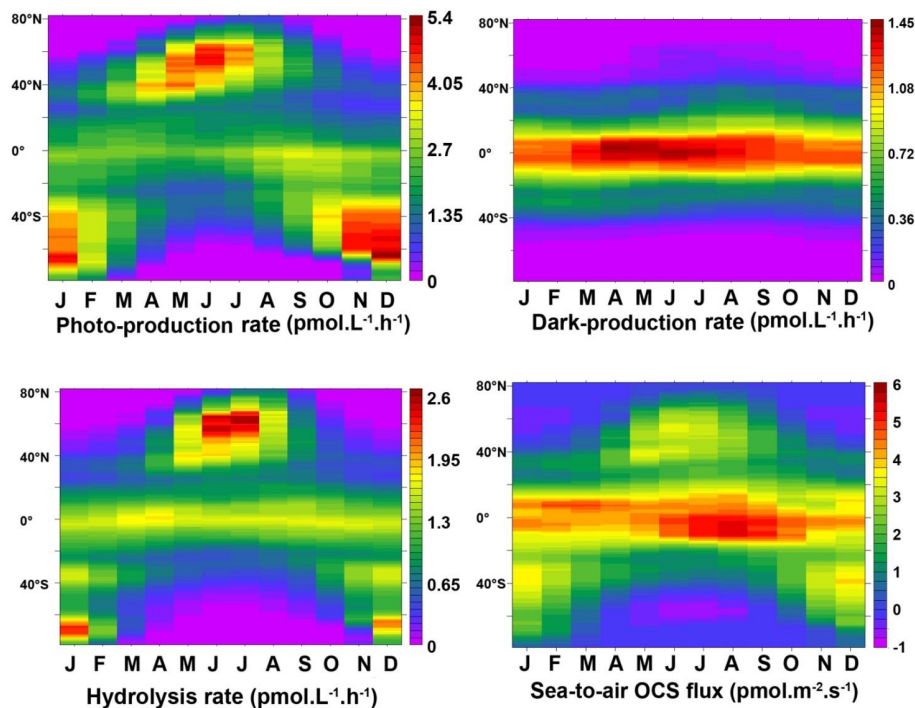


Figure 8. Latitude-time plots comparing relative importance of individual processes for OCS production (top row) and removal (bottom row) in NEMO-PISCES surface layer. Sea–air exchanges are displayed in bottom right panel are displayed with positive fluxes when OCS is outgassed towards the atmosphere. All runs were performed using Morel and Gentili (2009) formulation to calculate a_{350} and Elliott et al. (1989) formulation of hydrolysis constant.

Title Page

Abstract

Introduction

Conclusions

References

Tables

Figures

◀

▶

◀

▶

Back

Close

Full Screen / Esc

Printer-friendly Version

Interactive Discussion



A new model for the global biogeochemical cycle of carbonyl sulfide

T. Launois et al.

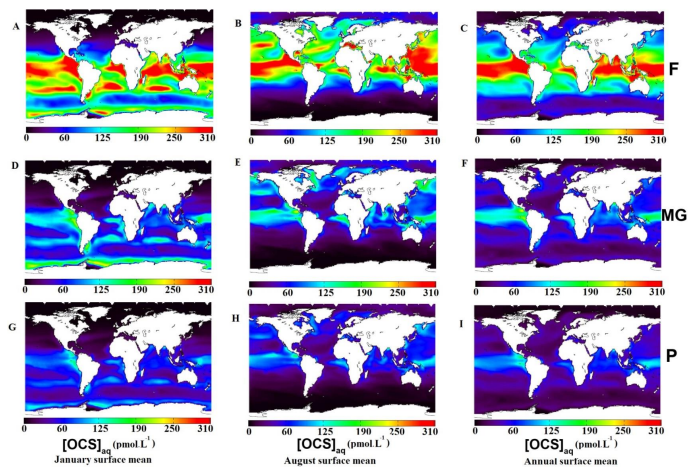


Figure 9. Monthly mean surface OCS concentrations for January (left column), August (central column) and annual mean (right column) simulated with NEMO-PISCES. The three simulations differ in the relationship used to calculate a_{350} from chlorophyll: MODIS Aqua -derived, proposed in this study (F, upper row), from Preiswerk et al. (2000) (P, central row) or Morel and Gentili (2009) (MG, lower row).

Title Page

Abstract

Introduction

Conclusions

References

Tables

Figures

◀

▶

◀

▶

Back

Close

Full Screen / Esc

Printer-friendly Version

Interactive Discussion



A new model for the global biogeochemical cycle of carbonyl sulfide

T. Launois et al.

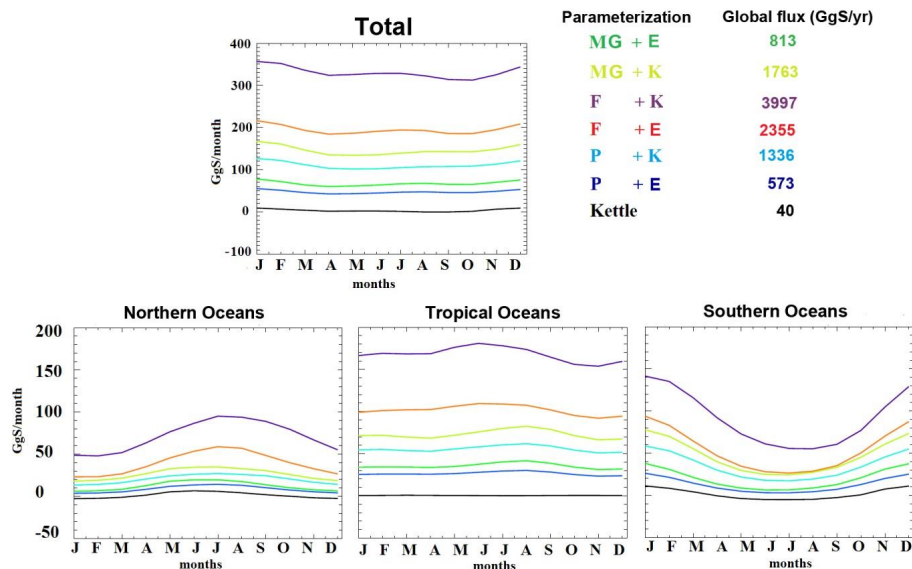


Figure 10. Global and regional monthly mean sea–air fluxes for 6 different parameterizations of the NEMO-PISCES model. Kettle et al. (2002) (black line) is shown as a reference. Each colored line represents a set of parameters: first name refers to the equation used to calculate the UV absorption coefficient of CDOM at 350 nm and the second name refers to the hydrolysis constant formulation. Global fluxes on top row, Northern Oceans (30–90° N, bottom left), Tropical region (30° S–30° N, bottom center), Southern Oceans (30–90° S, bottom right). F: a_{350} relation assembled in this study; MG: a_{350} relation from Morel and Gentili (2009); P: a_{350} relation from Preiswerk et al. (2000); E: hydrolysis constant from Elliott et al. (1989); K: hydrolysis constant from Kamyshny et al. (2003)

[Title Page](#)
[Abstract](#)
[Introduction](#)
[Conclusions](#)
[References](#)
[Tables](#)
[Figures](#)
[Back](#)
[Close](#)
[Full Screen / Esc](#)
[Printer-friendly Version](#)
[Interactive Discussion](#)